MSIGen: An Open-Source Python Package for Processing and Visualizing Mass Spectrometry Imaging Data

Emerson Hernly[a)], Hang Hu[a)], Julia Laskin[a)*]

a) Department of Chemistry, Purdue University, West Lafayette, Indiana, 47907, United States

*For correspondence and request for materials should be addressed to Dr. Julia Laskin

Email jlaskin@purdue.edu

ABSTRACT

Mass spectrometry imaging (MSI) provides information about the spatial localization of molecules in complex samples with high sensitivity and molecular selectivity. Although point-wise data acquisition, in which mass spectra are acquired at pre-defined points in a grid pattern, is common in MSI, several MSI techniques use line-wise data acquisition. In the line-wise mode, the imaged surface is continuously sampled along consecutive parallel lines and MSI data are acquired as a collection of line scans across the sample. Furthermore, aside from the standard imaging mode in which a full mass spectrum is acquired in each pixel of the image, other data acquisition modes have been developed to enhance the molecular specificity, enable separation of isobaric and isomeric species, and improve the sensitivity to facilitate imaging of low abundance species. These methods, including MS/MS-MSI in both MS^2 and MS^3 modes, multiple-reaction monitoring (MRM)-MSI, and ion mobility spectrometry (IMS)-MSI have all demonstrated their capabilities, but their broader implementation is limited by the existing MSI analysis software. Here, we present MSIGen, an open-source Python package for the visualization of MSI experiments performed in line-wise acquisition mode containing MS^1, MS^2, and IMS data. The package supports multiple vendor-specific and open-source data formats. It is available for download from the Python Package Index (PyPI) and its source-code is available at https://github.com/LabLaskin/MSIGen. This package contains tools for targeted extraction of ion images, and allows for normalization, and exportation as image arrays or publication-style images. MSIGen offers multiple interfaces allowing for accessibility and easy integration with other workflows. Considering its support for a wide variety of MSI imaging modes and vendor formats, MSIGen is a valuable tool for the visualization and analysis of MSI data.

Keywords

Mass spectrometry imaging; Data visualization; nano-DESI MSI; Python package; Open access software.

INTRODUCTION

Mass spectrometry imaging (MSI) is a powerful technique for label-free, spatially resolved chemical analysis of hundreds of molecules in the same experiment. (1–5) MSI has been applied to a diverse set of samples including plant (6,7) and animal tissues, (8,9) microbial and yeast colonies, (10,11) and surfaces prepared using ion soft-landing. (12,13) Most MSI experiments that rely on matrix assisted laser desorption ionization (MALDI) (14–16) or secondary ion mass spectrometry (SIMS) (17–19) use a pulsed laser or ion beam to desorb and ionize compounds from the sample. In these experiments, mass spectra are typically acquired in a point-wise fashion, meaning that each mass spectrum is collected at a predefined point on a grid and saved to the same file. MSI data are often converted into the commonly used open-source .imzML MSI file format, which is compatible with open-source software for data analysis including Cardinal, (20) Metaspace, (21) MSIQuant, (22) MzMine, (23) and rMSIproc. (24) Meanwhile, SCiLS (Bruker, Billerica, MA, USA) is one of the most widely used commercial software that supports point-wise data acquisition mode, with other options including MSIReader, (25) Mozaic MSI (Spectroswiss, Lausanne, Switzerland), (26) and more.

Several other ionization techniques used in MSI experiments including desorption electrospray ionization (DESI), (27) nanospray-desorption electrospray ionization (nano-DESI), (28) and scanning probe electrospray ionization (sPESI) (29) rely on data acquisition performed in a line-wise fashion. In this mode, line scans are acquired across the sample, and each line is saved as a separate file. Currently, there is limited software available for visualizing data acquired using the line-wise data acquisition mode. Free and open-source tools that support this mode include Ion-to-Image (i2i) (30) and MSIQuickView. (31,32) i2i can effectively visualize data from Thermo Fisher Scientific (Waltham, MA, USA) instruments containing MS data with arbitrary numbers of activation events after conversion to .mzML format. MSIQuickView is more limited, only supporting MSI data containing MS^1 or MS/MS (MS^2) spectra and is no longer maintained. Mozaic MSI is a commercial program that supports both point-wise and line-wise data acquisition modes and has been used for visualizing nano-DESI MSI data. (26,33,34)

Typical MSI experiments are acquired using the full MS^1 mode. Meanwhile, other acquisition modes, including ion mobility spectrometry (IMS)-MSI, (35–41), multiple-reaction monitoring (MRM)-MSI, (42,43) MS^2-MSI, (44–47) and MS^3-MSI (48,49) have demonstrated their power by enabling better separation of the isobaric and isomeric species in complex lipid and metabolite mixtures extracted during MSI of biological samples. Despite the advantages provided by these acquisition modes, they are rarely implemented due to software limitations. Current software including i2i, MSIQuickView, SCiLS, and Mozaic all support MS^2-MSI. However, they are often limited to specific data formats and do not support all the acquisition modes described earlier. Furthermore, none of them currently support line-wise acquisition IMS-MSI data, and neither of the open-source software support the visualization of data from multiple instrument vendors. An open-source IMS-MSI data processing workflow (50) developed to address

challenges associated with the visualization of IMS-MSI data uses several platforms and is difficult to maintain.

To address this challenge, we have developed MSIGen, an open-source Python package that can visualize line-wise MSI data files and save them in either image or array formats. MSIGen supports MS^1, MS^2, MRM, and IMS-MSI data in the open-source .mzML format or commercial file formats, including those used by Agilent (Santa Clara, CA, USA), Thermo Fisher (Waltham, MA, USA), and timsTOF instruments from Bruker (Billerica, MA, USA). We provide an option to use a graphical user interface (GUI), Jupyter Notebook, or command line interface, which significantly simplifies data visualization and makes this package flexible and easy to adapt to new modes of data acquisition.

MATERIALS AND METHODS

A Windows 10 laptop containing an Intel Core 17-7700HQ and 16 GB of RAM with a 1TB HGST HDD hard drive was used for the development and testing of MSIGen. The package was developed in Python 3.9 and is currently compatible with Windows and Python versions 3.9-3.11. The following packages are used as dependencies: Multiplierz, (51) pymzML, (52) OpenTimsPy, (53) NumPy, (54) Pandas, (55) SciPy, (56) scikit-image, (57) Matplotlib, (58) pywin32, Numba, (59) and tqdm. (60) A script and .dll to access Bruker's .tsf format data was provided by Bruker (Billerica, MA, USA). Any file conversion to the .mzML format was done with MSConvert v3.0.23054-b585bc2. (61)

Table 1. A list of datasets used for the development and testing of MSIGen

Dataset	Instrument	Data Content	Size (MB)	Number of Line scans
1 (ref. 44)	Q-Exactive HF-X Orbitrap	MS^1	1328	65
2 (ref. 62)	Q-Exactive HF-X Orbitrap	MS^2	636	39
3 (ref. 43)	Agilent 6560 IM-QTOF	MS^1	1875	51
4 (ref. 63)	Agilent 6560 IM-QTOF	IMS- MS^1	6840	56
5 (ref. 43)	Agilent Ultivo triple quadrupole	MRM	94	46
6 (ref. 64)	TimsTOF Pro2	MS^1	489	38
7 (ref. 36)	TimsTOF Pro2	IMS- MS^1	783	37

Experimental details of each dataset can be found in their respective publications. (36,43,44,62–64) As indicated in Table 1, these datasets were acquired on a Thermo Fisher Q-Exactive HF-X Orbitrap MS, Agilent 6560 IM-QTOF MS, Bruker timsTOF Pro2 MS, and Agilent Ultivo triple quadrupole MS. Each experiment used a custom nano-DESI source, described elsewhere. (28,31,36,43,47,63–68) Data were collected in multiple reaction monitoring (MRM) mode for the Agilent Ultivo triple quadrupole MS, while all other instruments used either full MS^1, MS^1-IMS, or MS^2 modes. In some experiments that included more than one scan type, different MS^1, MRM, or MS^2 scans were acquired sequentially, and then repeated in a cycle. Multiple line

scans were acquired by moving the sample stage under the nano-DESI probe while acquiring mass spectra. Each mass spectrum in the line scan represents one pixel in the ion image and each line scan is saved as a separate file. Most datasets had some amount of variation in the number of MS spectra per line scan. This is more pronounced in the MSI data acquired using Q-Exactive HF-X Orbitrap MS, which uses automatic gain control (AGC). AGC automatically adjusts the ion injection time to reduce the space charge effect, which results in variations in the acquisition time between mass spectra. (69)

RESULTS AND DISCUSSION

MSIGen, available as a Python package (https://github.com/LabLaskin/MSIGen), enables easy and accessible image generation and exportation. This package offers tools for user file and parameter input, image array creation, image normalization, and image visualization. The visualization tool supports the generation of ion images from datasets that include MS^1, MRM, and MS^2 spectra, with or without IMS separation. In addition, fractional images and ratio images can be generated. In fractional images, ion signals in each pixel of the image are divided by the sum of that pixel from multiple ion images. Meanwhile, ratio images are generated by dividing one ion image by another. Images can be viewed using a variety of colormaps offered by Matplotlib (58). Additionally, very bright pixels can be dimmed using a spike handling tool. This reduces the intensity of the bright pixel to that of the user-provided *n*th quantile of the intensities within each image. Publication-style images (as .png, .jpeg, or .tiff) can be exported with automatically generated descriptive titles or with user-provided titles.

Table 2 displays the file types that are supported by MSIGen alongside the package that is used to read each file type. MSIGen directly supports MS^1, MRM, and MS^2 data in .mzML files and multiple commercial formats including .raw from Thermo Fisher, .d from Agilent, and .d from Bruker timsTOF instruments. IMS data in .mzML files and .d files from Bruker timsTOF instruments are also supported. Other files that are not directly supported can be converted using MSConvert to .mzML format, and subsequently imported into MSIGen. (61)

Table 2. Summary of supported file types in MSIGen and the file reader for each

File Format	IMS support	MS File Reader
.raw (Thermo Fisher)	No	Multiplierz (51)
.d (Agilent)	No	Multiplierz (51)
.d files in .tsf or .tdf format (Bruker timsTOF instruments)	Yes	tsf.py (.tsf) or OpenTimsPy (53) (.tdf)
.mzML (From MSConvert)	Yes	pymzML

Vendor formats not shown in Table 2 were not tested, so they may or may not be supported by conversion to .mzML format. Due to issues with MSConvert, files from Agilent triple quadrupole

instruments are only accessible directly as .d files and not after conversion to .mzML format. Additionally, the current version of MSIGen assumes that only one MS^1 mass window is present in the data and therefore it does not support files with multiple MS^1 windows.

Data processing workflows.

The MSIGen workflow differs depending on the experiment type, which can be MS^1, MS^2, MS^1-IMS, and MS^2-IMS. Additionally, the workflow differs slightly for each accepted file type shown in Table 2. The main difference in workflow between file types is that the reader for the MS files differs. The MS file readers used for each file type are specified in Table 2.

The MS^1 workflow for MSIGen begins with the user providing the paths of the MS files, a mass list (as .xlsx or .csv) containing relevant *m/z* values also referred to as transition list, and other user-defined parameters such as mass tolerance and the dimensions of the imaged area. Details about the mass list can be found in Table S1. MSIGen loads the MS line scan files sequentially and extracts the intensity values for all mass list entries from each contained mass spectrum. Intensities are obtained by summing the intensities of all data points that are within the specified *m/z* tolerance window. For each line, intensities are saved to an array of shape *(n, s)* where *n* is the number of mass list entries plus one for the total ion count (TIC), and *s* is the number of spectra in the line. Additionally, the time point at which each spectrum was acquired is recorded. Since the time point of each spectrum is directly related to the position at which the spectrum was acquired, the time point can be used to determine the location of the spectrum in the image. Due to the variations in the spectrum acquisition rate, the time point of each spectrum differs across lines and the number of spectra in each line may differ. MSIGen uses nearest-neighbor interpolation to resample each line scan at uniformly separated points to generate an array of signals with the same number of spectra per line and aligned time points across all lines. After resampling, the data is saved as an image array of shape (*n, x, y*) where *x* is the number of line scans, and *y* is the greatest number of spectra in a single line scan. This array is saved as a .npy or .csv file. Input parameters, the mass list entries, and relevant instrumental data are saved in a separate file.

For the MS^1-IMS workflow, the only significant difference compared to the MS^1 workflow is that intensities are obtained by summing the intensity of all data within both an *m/z* and an ion mobility tolerance window.

For MS^2-MSI and MRM-MSI data, the workflow begins with a preprocessing step, which groups mass spectra based on their *m/z* range, precursor, scan type (ex. MS^1, MS^2, etc.), and polarity. Entries in the mass list are then grouped into transition groups if they appear in the same set of spectra, as shown in Figure S1. To prevent slow processing times, the length of the line arrays must be equal to the number of spectra in the line. However, it is likely that each transition group has a different number of spectra in each line. Therefore, a line array is saved for each transition group. Two *m/z* tolerance windows are used to extract signal from MS^2 spectra: one for the precursor and one for the fragment. The images are by default saved as a single array. In this

process, each line is resampled similarly to the MS^1 workflow. Alternatively, the images can be saved as multiple arrays, one for each transition group. Here each line array is resampled at x uniformly separated points, where x is the greatest number of spectra of the transition group in a single line. Saving as a single image array simplifies subsequent data processing, while one array for each transition group reduces distortion due to resampling during interpolation.

The MS^2-IMS workflow follows the MS^2 workflow but uses the ion mobility window of each spectrum as another factor to group spectra and transitions. It also uses an ion mobility tolerance window in addition to the precursor and fragment *m/z* tolerance windows to obtain intensity values.

GUI Interface for MSIGen

There are three options to interface with MSIGen: a guided user interface (GUI), Jupyter notebook interface, or command line interface. All interfaces provide the same outputs, but the GUI is easiest to use for those with no coding experience. Meanwhile, the Jupyter notebook offers interactivity and better control over the visualization parameters, and the command line interface enables the development of automated workflows.

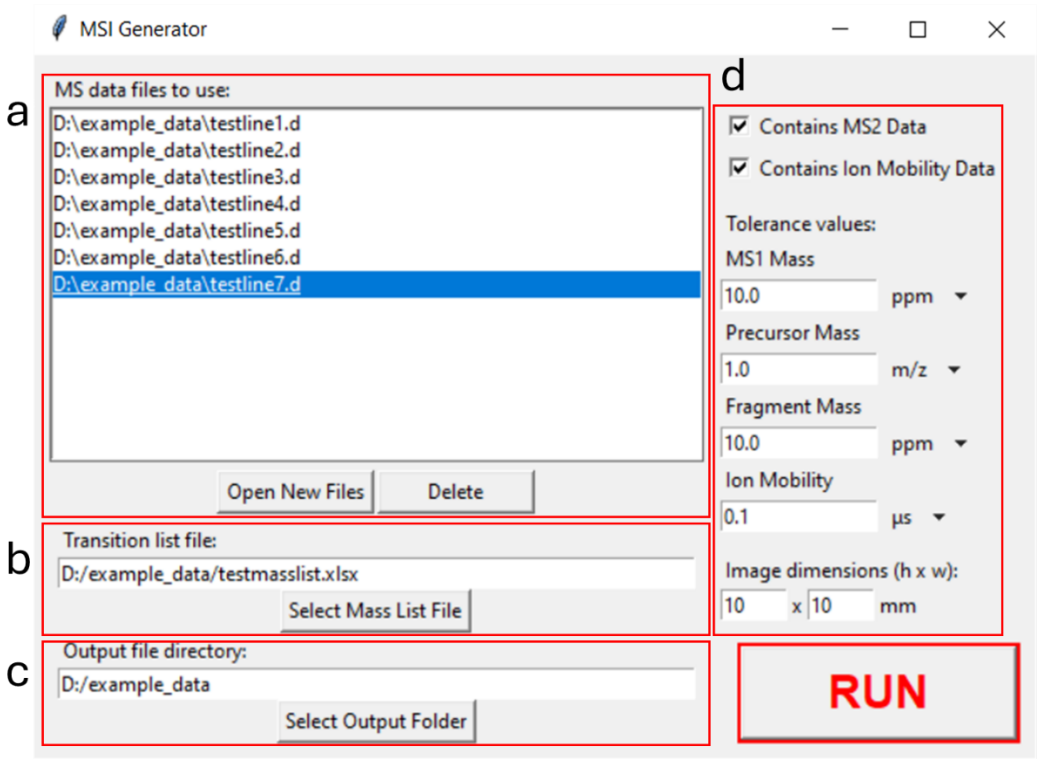

Figure 1. The main window of the MSIGen GUI contains fields for (a) selected files, (b) file path for the transition list, (c) folder to save output files to. Data processing parameters including the values of all tolerances and the spatial dimensions of the imaged area are specified in (d). This panel also allows the user to specify whether the MS files contain MS^2 scans or any IMS data. The "Run" button begins data processing.

The main window of the GUI, shown in Figure 1, prompts the user to input the paths for the MS line scan files, the mass list, and the output directory. In addition, checkboxes are used to indicate whether the MS files contain MS^2 or ion mobility data. For the purposes of MSIGen, files are considered to contain MS^2 data if either full MS^2 scans or MRM data are present. Other parameters such as tolerance values and the dimensions of the imaged area must also be defined. For ease of use, the user can provide the paths for all MS files, or a single MS file path, in which case MSIGen automatically finds the other line scan files, as shown in Figure S2. Pressing the "RUN" button opens a progress bar and starts the image extraction process.

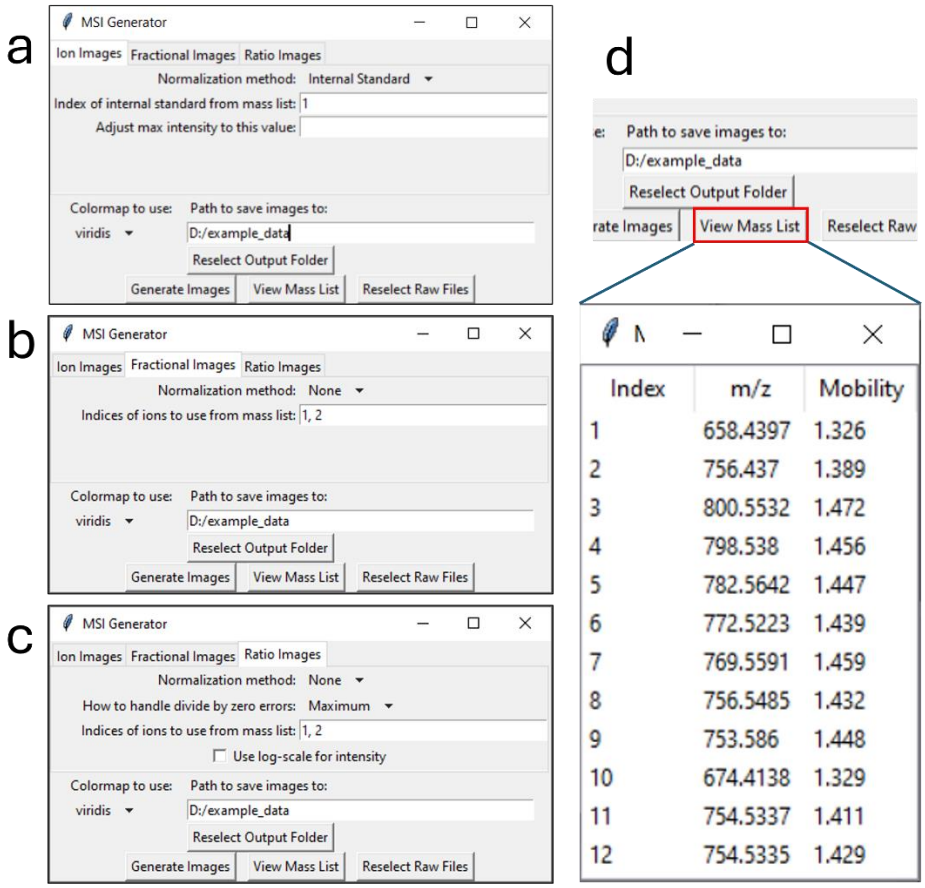

Figure 2. The image creation window with (a) the ion image page, (b) the fractional image page, and (c) the ratio image page. (d) Clicking the "View Mass List" button displays the mass list entries alongside their index, which are used in entry boxes in (a) (b) and (c).

Next, the image creation window shown in Figure 2 will appear. This window contains three tabs, in which the user specifies parameters for generating ion images, fractional images, or ratio images. In each of the tabs, the mode of normalization, output directory, and color maps are specified. Ion images can be saved as raw images or can be normalized to the TIC or an internal standard as shown in Figure 3. To support the generation of different types of ion images, each *m/z*

window is assigned an index based on the order of the mass list file. To generate ion images without any normalization (raw images) or TIC normalization, the user must simply specify the normalization method. To generate ion images normalized to the internal standard, the index of the internal standard must be specified. The index can be found by opening the mass list using the "View Mass List" button.

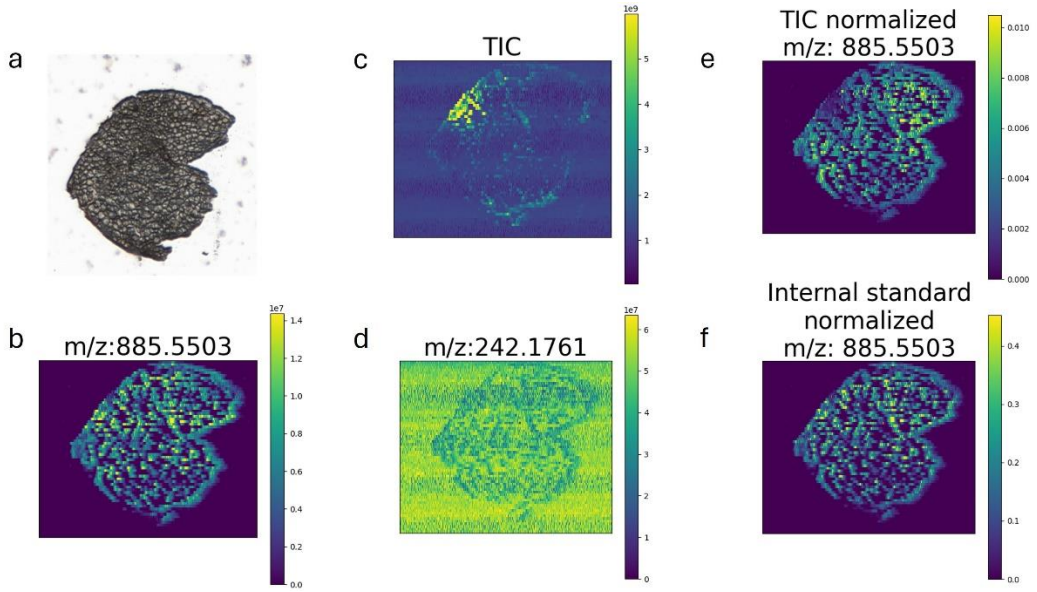

Figure 3. (a) The optical image of the mouse muscle tissue section imaged in dataset #1. (b) The ion image of an endogenous species at *m/z* = 885.5503; (c) the TIC image; (d) the ion image of the internal standard at *m/z* = 242.1761; (e) the ion image of *m/z* = 885.5503 normalized to TIC; (f) the ion image of *m/z* = 885.5503 normalized to the internal standard. The *m/z* tolerance to generate these images was ±10 ppm. The colormap used to generate these images is viridis.

The generation of fractional and ratio images is illustrated. Figure 4 shows a comparison of the spatial localizations of isobaric species in experiment #4, which contains IMS-MSI data. The fractional images in Figure 4c can be generated by specifying the indices of the images to be used, separated by commas. Each image is divided by the sum of all the images for which the index was provided. Fractional images can be base peak normalized, where all images are normalized to the signal in their brightest pixel before summation and division. This normalization option enables better comparison of the spatial distribution of images with intensities that differ substantially.

Ratio images, seen in Figure 4d, are generated by providing the indices of the two images that will be used. These can be base peak normalized the same as fractional images and can be displayed using a log scale for intensity. MSIGen offers the option to replace divide-by-zero errors with zero, infinity, or the maximum of the ratio image. Pressing "Generate Images" saves publication style images using one of a variety of colormaps, and a link to the save location will appear when complete. Overall, MSIGen's visualization tool enables users to obtain images of ion,

fractional, or ratio images with multiple normalization options to allow for direct or comparative visualization of the spatial distributions of analytes.

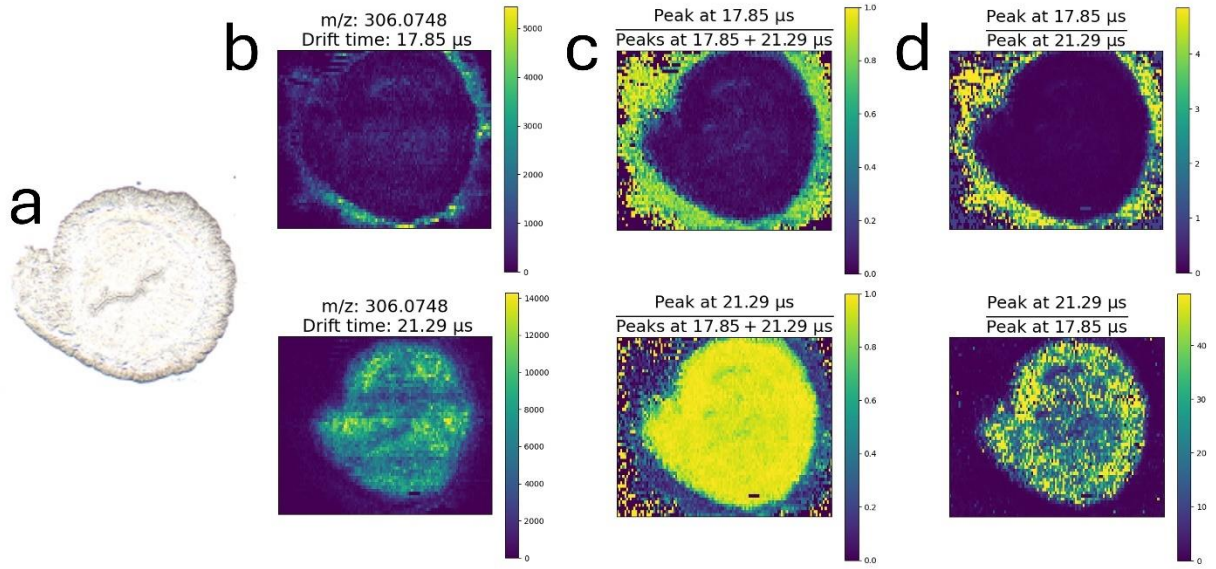

Figure 4. IMS-MSI images of two species with the *m/z* value of 306.0748 and differing ion mobility values of 17.85 µs and 21.29 µs from dataset #4. (a) The optical microscopy image of the mouse uterine section. (b) Unnormalized ion images of the two species. The spatial distributions of these two species were compared by generating (c) fractional images and (d) ratio images. All images were generated using the MSIGen Jupyter notebook using a *m/z* tolerance of ±10 ppm and a mobility tolerance of ±0.5 µs.

MSIGen Jupyter Notebook Interface

Jupyter notebook is an interactive Python kernel that allows for running small portions of the code at a time, making it easy to use for step-by-step processes. The Jupyter notebook made for MSIGen offers expanded functionality compared to the GUI. Rather than requiring intensity extraction from MS files before proceeding to the visualization step, the Jupyter notebook can load previously generated image arrays, which substantially reduces the time needed to export images. The Jupyter notebook can also be saved including all the user-specified input parameters. This allows the user to re-process the dataset without specifying the parameters again. The Jupyter notebook also offers more options during image visualization, such as displaying images before saving them, displaying only a few rather than all images, adding user-provided titles to the images, and allowing the user to change the aspect ratio of the pixels more easily. Additionally, the internal standard can be defined based on its *m/z* and mobility values instead of finding its index from the mass list.

MSIGen Command Line Interface

The command line interface for MSIGen allows the user to process and save images for multiple experiments without further input after starting. The command line interface requires that parameters are provided within .json format configuration files. Running the MSIGen_CLI.py file with the paths to the configuration files as arguments consecutively extracts and saves images for each provided file. Since these configurations files are relatively simple, they can be procedurally generated, allowing for users to easily include MSIGen in their own automated workflows.

MSIGen Performance

Each of the datasets was converted to .mzML except for the Agilent Ultivo triple quadrupole dataset, which cannot be converted properly by MSConvert. All compatible files were processed using MSIGen, with relevant data recorded in Table 3.

Table 3. Summary of each dataset and its processing time in MSIGen

Dataset from Table 1	File format	Data Content	Size (MB)	Number of Lines	Number of Mass List Entries	Processing Time (s)
1	.raw	MS^1	1328	65	507	106
1	.mzML	MS^1	3698	65	507	336
2	.raw	MS^2	577	39	41	49
2	.mzML	MS^2	1766	39	41	83
3	.d (Agilent)	MS^1	1875	51	500	30
3	.mzML	MS^1	8256	51	500	75
4	.mzML	IMS-MS^1	40329	56	7	33min 30s
5	.d (Agilent)	MRM	17.4	6	8	231
6	.d (Bruker .tsf)	MS^1	489	9	164	90
6	.mzML	MS^1	4477	9	164	351
7	.d (Bruker .tdf)	IMS-MS^1	783	37	12	48
7	.mzML	IMS-MS^1	2003	37	12	293

For each data set, we compared the processing time for the original files in vendor-specific formats and data converted to the .mzML format. The files were converted using MSConvert with and default settings apart from turning “combine ion mobility scans” on. It is apparent from Table 3 that the processing times for .mzML files are much slower than for the commercial file formats. For all the datasets that we compared, it took at least 1.7 times longer to process them as .mzML files, with dataset #7 taking more than 6 times longer. These results highlight the benefits of MSIGen directly supporting commercial data formats, especially when considering the time needed to convert the files to .mzML format.

However, MSConvert has options to reduce the size of converted .mzML files, which also reduces the processing time in MSIGen. We used dataset #7 to compare the effect of different conversion settings on the processing time. The results of this comparison are summarized in table

4. We found that three settings contribute to a significant reduction in processing time. Specifically, decreasing the encoding precision from the default 64-bit to 32-bit results in a more than 5-fold decrease in processing time. It also reduces the space needed to save the .mzML files. Using a peak-picking algorithm, the vendor-provided option in this case, results in a minor decrease in processing time. Using a threshold peak filter to keep only peaks over a user specified intensity threshold or instead to keep the top user-specified *n* peaks can also substantially reduce processing time and file size. However, care should be taken when using a threshold peak filter as it can remove low intensity signals from the dataset if the thresholds are too high or keep too few peaks.

Table 4. Processing time for dataset #7 after conversion to .mzML format using varying settings.

Encoding precision	**Peak picking filter**	**Threshold peak filter**	**Size (MB)**	**Processing Time (s)**
64-bit	None	None	2003	293
32-bit	None	None	1278	35
32-bit	Vendor	None	1279	34
32-bit	Vendor	Keep peaks with >10 absolute intensity	655	22
32-bit	Vendor	Keep top 100 peaks	27	5

Next, dataset #1 was converted to .mzML format using a 32-bit encoding and no peak picking or threshold peak filter. This dataset was processed multiple times, each time with mass lists of different size. As seen in Figure 5, the relationship between the number of mass entries and processing time is linear with a large y-intercept. This is expected, since there is a substantial overhead when loading and reading the .mzML files, indicating potential for further improvement in processing speed.

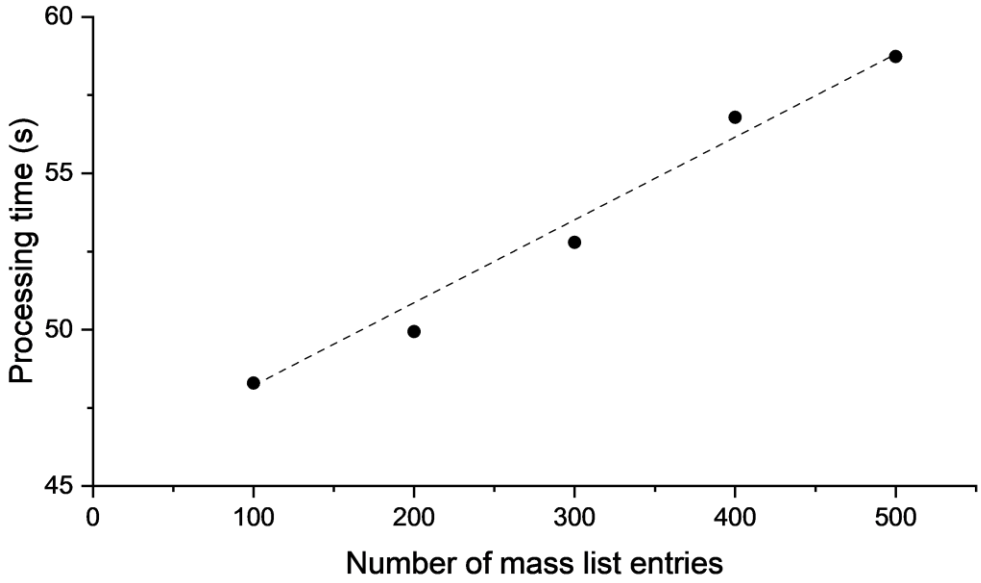

Figure 5. Processing time for dataset #1 as a function of the number of *m/z* windows extracted. The dataset was acquired on a Q-Exactive HF-X Orbitrap and contains MS^1 data. It is an 1878 MB .mzML file with 32-bit encoding precision. The plot is relatively linear, with a coefficient of determination (R^2) equal to 0.9819.

Because MSIGen can process even very large datasets such as dataset #4 on a laptop, it should be compatible with most laboratory Windows machines and standard imaging datasets. Overall, MSIGen provides acceptable processing times for applications that do not require real-time monitoring, particularly when using supported commercial data formats and or 32-bit encoding precision .mzML files. Nevertheless, there is room for future optimization of MSIGen through multithreading and updates to dependencies.

CONCLUSIONS

We have developed MSIGen, an open-source Python package for the visualization and analysis of MSI data acquired in a line-wise fashion. MSIGen supports multiple MSI modes, including IMS-MSI, MS^2-MSI, and MRM-MSI. The software accepts multiple open-source and commercial formats making it widely applicable. The visualization tool can be used to generate ion, fractional, and ratio images with different types of normalization. The extracted images can also be exported into arrays for further analysis. MSIGen offers a GUI, Jupyter Notebook, and command line interface to interact with the package, allowing for flexible application and adaptation to user workflows. Overall, MSIGen fills the need for a MSI visualization program that is not limited to specific instruments and that can accept multiple MSI modes, most notably IMS-MSI, MS^2-MSI, and MRM-MSI. This development will facilitate the adaptation of these or other modes of MSI data acquisition that will further enhance the specificity, sensitivity, and molecular identification capabilities of MSI.

Author Information

Corresponding author

Julia Laskin - Department of Chemistry, Purdue University, West Lafayette, Indiana, 47907, United States; https://orcid.org/0000-0002-4533-9644; Email: Jlaskin@purdue.edu

Authors

Emerson Hernly - Department of Chemistry, Purdue University, West Lafayette, Indiana, 47907, United States; https://orcid.org/0009-0009-6374-3761

Hang Hu - Department of Chemistry, Purdue University, West Lafayette, Indiana, 47907, United States. https://orcid.org/0000-0002-8590-9787

ACKNOWLEDGMENTS

This work was partially supported by grants from the National Science Foundation (2108729, 2333734, and IIP-1916691) and National Institutes of Health (RF1MH128866 and UH3CA255132). We would like to thank those who acquired the data used to develop MSIGen: Lixue Jiang, (Purdue University, West Lafayette, IN) Miranda Weigand, (Purdue University, West Lafayette, IN) and Daisy Unsihuay (University of Pennsylvania, Philadelphia, PA). We also thank Dr. Heiko Neuweger (Bruker Daltonics, Bremen, Germany) for providing assistance and the materials needed to access Bruker data files. The authors also acknowledge David Helminiak (Department of Electrical and Computer Engineering, Marquette University, Milwaukee, WI) and Maxwell Alexander (Alexander Bioinformatics, Cambridge, MA) for their support in updating multiplierz to be compatible with MSIGen.

REFERENCES

(1) Chaurand, P.; Schwartz, S. A.; Reyzer, M. L.; Caprioli, R. M. Imaging Mass Spectrometry: Principles and Potentials. *Toxicol Pathol* **2005**, *33* (1), 92–101. https://doi.org/10.1080/01926230590881862.

(2) Amstalden van Hove, E. R.; Smith, D. F.; Heeren, R. M. A. A Concise Review of Mass Spectrometry Imaging. *Journal of Chromatography A* **2010**, *1217* (25), 3946–3954. https://doi.org/10.1016/j.chroma.2010.01.033.

(3) Rae Buchberger, A.; DeLaney, K.; Johnson, J.; Li, L. Mass Spectrometry Imaging: A Review of Emerging Advancements and Future Insights. *Anal Chem* **2018**, *90* (1), 240–265. https://doi.org/10.1021/acs.analchem.7b04733.

(4) Spengler, B. Mass Spectrometry Imaging of Biomolecular Information. *Anal. Chem.* **2015**, *87* (1), 64–82. https://doi.org/10.1021/ac504543v.

(5) Wu, C.; Dill, A. L.; Eberlin, L. S.; Cooks, R. G.; Ifa, D. R. Mass Spectrometry Imaging under Ambient Conditions. *Mass Spectrometry Reviews* **2013**, *32* (3), 218–243. https://doi.org/10.1002/mas.21360.

(6) Bjarnholt, N.; Li, B.; D'Alvise, J.; Janfelt, C. Mass Spectrometry Imaging of Plant Metabolites – Principles and Possibilities. *Natural Product Reports* **2014**, *31* (6), 818–837. https://doi.org/10.1039/C3NP70100J.

(7) Lee, Y. J.; Perdian, D. C.; Song, Z.; Yeung, E. S.; Nikolau, B. J. Use of Mass Spectrometry for Imaging Metabolites in Plants. *The Plant Journal* **2012**, *70* (1), 81–95. https://doi.org/10.1111/j.1365-313X.2012.04899.x.

(8) Chughtai, K.; Heeren, R. M. A. Mass Spectrometric Imaging for Biomedical Tissue Analysis. *Chem. Rev.* **2010**, *110* (5), 3237–3277. https://doi.org/10.1021/cr100012c.

(9) Arentz, G.; Mittal, P.; Zhang, C.; Ho, Y.-Y.; Briggs, M.; Winderbaum, L.; Hoffmann, M. K.; Hoffmann, P. Chapter Two - Applications of Mass Spectrometry Imaging to Cancer. In *Advances in Cancer Research*; Drake, R. R., McDonnell, L. A., Eds.; Applications of Mass Spectrometry Imaging to Cancer; Academic Press, 2017; Vol. 134, pp 27–66. https://doi.org/10.1016/bs.acr.2016.11.002.

(10) Fang, J.; Dorrestein, P. C. Emerging Mass Spectrometry Techniques for the Direct Analysis of Microbial Colonies. *Current Opinion in Microbiology* **2014**, *19*, 120–129. https://doi.org/10.1016/j.mib.2014.06.014.

(11) Dunham, S. J. B.; Ellis, J. F.; Li, B.; Sweedler, J. V. Mass Spectrometry Imaging of Complex Microbial Communities. *Acc. Chem. Res.* **2017**, *50* (1), 96–104. https://doi.org/10.1021/acs.accounts.6b00503.

(12) Samayoa-Oviedo, H. Y.; Behrend, K.-A.; Kawa, S.; Knorke, H.; Su, P.; Belov, M. E.; Anderson, G.; Warneke, J.; Laskin, J. Design and Performance of a Soft-Landing Instrument for Fragment Ion Deposition. *Anal. Chem.* **2021**, *93* (43), 14489–14496. https://doi.org/10.1021/acs.analchem.1c03009.

(13) Gholipour-Ranjbar, H.; Samayoa-Oviedo, H. Y.; Laskin, J. Controlled Formation of Fused Metal Chalcogenide Nanoclusters Using Soft Landing of Gaseous Fragment Ions. *ACS Nano* **2023**, *17* (17), 17427–17435. https://doi.org/10.1021/acsnano.3c05545.

(14) Gessel, M. M.; Norris, J. L.; Caprioli, R. M. MALDI Imaging Mass Spectrometry: Spatial Molecular Analysis to Enable a New Age of Discovery. *Journal of Proteomics* **2014**, *107*, 71–82. https://doi.org/10.1016/j.jprot.2014.03.021.

(15) Cornett, D. S.; Reyzer, M. L.; Chaurand, P.; Caprioli, R. M. MALDI Imaging Mass Spectrometry: Molecular Snapshots of Biochemical Systems. *Nat Methods* **2007**, *4* (10), 828–833. https://doi.org/10.1038/nmeth1094.
(16) Francese, S.; Dani, F. R.; Traldi, P.; Mastrobuoni, G.; Pieraccini, G.; Moneti, G. MALDI Mass Spectrometry Imaging, from Its Origins up to Today: The State of the Art. *Combinatorial Chemistry & High Throughput Screening* **2009**, *12* (2), 156–174. https://doi.org/10.2174/138620709787315454.
(17) Passarelli, M. K.; Winograd, N. Lipid Imaging with Time-of-Flight Secondary Ion Mass Spectrometry (ToF-SIMS). *Biochimica et Biophysica Acta (BBA) - Molecular and Cell Biology of Lipids* **2011**, *1811* (11), 976–990. https://doi.org/10.1016/j.bbalip.2011.05.007.
(18) Fletcher, J. S.; Vickerman, J. C.; Winograd, N. Label Free Biochemical 2D and 3D Imaging Using Secondary Ion Mass Spectrometry. *Current Opinion in Chemical Biology* **2011**, *15* (5), 733–740. https://doi.org/10.1016/j.cbpa.2011.05.016.
(19) Massonnet, P.; A. Heeren, R. M. A Concise Tutorial Review of TOF-SIMS Based Molecular and Cellular Imaging. *Journal of Analytical Atomic Spectrometry* **2019**, *34* (11), 2217–2228. https://doi.org/10.1039/C9JA00164F.
(20) Bemis, K. D.; Harry, A.; Eberlin, L. S.; Ferreira, C.; van de Ven, S. M.; Mallick, P.; Stolowitz, M.; Vitek, O. Cardinal: An R Package for Statistical Analysis of Mass Spectrometry-Based Imaging Experiments. *Bioinformatics* **2015**, *31* (14), 2418–2420. https://doi.org/10.1093/bioinformatics/btv146.
(21) Palmer, A.; Phapale, P.; Chernyavsky, I.; Lavigne, R.; Fay, D.; Tarasov, A.; Kovalev, V.; Fuchser, J.; Nikolenko, S.; Pineau, C.; Becker, M.; Alexandrov, T. FDR-Controlled Metabolite Annotation for High-Resolution Imaging Mass Spectrometry. *Nat Methods* **2017**, *14* (1), 57–60. https://doi.org/10.1038/nmeth.4072.
(22) Källback, P.; Nilsson, A.; Shariatgorji, M.; Andrén, P. E. msIQuant – Quantitation Software for Mass Spectrometry Imaging Enabling Fast Access, Visualization, and Analysis of Large Data Sets. *Anal. Chem.* **2016**, *88* (8), 4346–4353. https://doi.org/10.1021/acs.analchem.5b04603.
(23) Schmid, R.; Heuckeroth, S.; Korf, A.; Smirnov, A.; Myers, O.; Dyrlund, T. S.; Bushuiev, R.; Murray, K. J.; Hoffmann, N.; Lu, M.; Sarvepalli, A.; Zhang, Z.; Fleischauer, M.; Dührkop, K.; Wesner, M.; Hoogstra, S. J.; Rudt, E.; Mokshyna, O.; Brungs, C.; Ponomarov, K.; Mutabdžija, L.; Damiani, T.; Pudney, C. J.; Earll, M.; Helmer, P. O.; Fallon, T. R.; Schulze, T.; Rivas-Ubach, A.; Bilbao, A.; Richter, H.; Nothias, L.-F.; Wang, M.; Orešič, M.; Weng, J.-K.; Böcker, S.; Jeibmann, A.; Hayen, H.; Karst, U.; Dorrestein, P. C.; Petras, D.; Du, X.; Pluskal, T. Integrative Analysis of Multimodal Mass Spectrometry Data in MZmine 3. *Nat Biotechnol* **2023**, *41* (4), 447–449. https://doi.org/10.1038/s41587-023-01690-2.
(24) Ràfols, P.; Heijs, B.; Del Castillo, E.; Yanes, O.; McDonnell, L. A.; Brezmes, J.; Pérez-Taboada, I.; Vallejo, M.; García-Altares, M.; Correig, X. rMSIproc: An R Package for Mass Spectrometry Imaging Data Processing. *Bioinformatics* **2020**, *36* (11), 3618–3619. https://doi.org/10.1093/bioinformatics/btaa142.
(25) Robichaud, G.; Garrard, K. P.; Barry, J. A.; Muddiman, D. C. MSiReader: An Open-Source Interface to View and Analyze High Resolving Power MS Imaging Files on Matlab Platform. *J. Am. Soc. Mass Spectrom.* **2013**, *24* (5), 718–721. https://doi.org/10.1007/s13361-013-0607-z.
(26) Huffstutler, C. D.; Sanchez, D. M.; Weigand, M. R.; Hu, H.; Li, X.; Chegwidden, A. J.; Nagornov, K. O.; Kozhinov, A. N.; Tsybin, Y. O.; Laskin, J. Multiple Selected Ion

Monitoring Mode for Sensitive Imaging of Eicosanoids in Tissues Using Nanospray Desorption Electrospray Ionization (Nano-DESI) Mass Spectrometry. *International Journal of Mass Spectrometry* **2023**, *491*, 117101. https://doi.org/10.1016/j.ijms.2023.117101.

(27) Takáts, Z.; Wiseman, J. M.; Gologan, B.; Cooks, R. G. Mass Spectrometry Sampling Under Ambient Conditions with Desorption Electrospray Ionization. *Science* **2004**, *306* (5695), 471–473. https://doi.org/10.1126/science.1104404.

(28) Roach, P. J.; Laskin, J.; Laskin, A. Nanospray Desorption Electrospray Ionization: An Ambient Method for Liquid-Extraction Surface Sampling in Mass Spectrometry. *Analyst* **2010**, *135* (9), 2233–2236. https://doi.org/10.1039/C0AN00312C.

(29) Otsuka, Y.; Shide, S.; Naito, J.; Kyogaku, M.; Hashimoto, H.; Arakawa, R. Scanning Probe Electrospray Ionization for Ambient Mass Spectrometry. *Rapid Communications in Mass Spectrometry* **2012**, *26* (23), 2725–2732. https://doi.org/10.1002/rcm.6399.

(30) Lillja, J.; Duncan, K. D.; Lanekoff, I. Ion-to-Image, I2i, a Mass Spectrometry Imaging Data Analysis Platform for Continuous Ionization Techniques. *Anal. Chem.* **2023**, *95* (31), 11589–11595. https://doi.org/10.1021/acs.analchem.3c01615.

(31) Lanekoff, I.; Heath, B. S.; Liyu, A.; Thomas, M.; Carson, J. P.; Laskin, J. Automated Platform for High-Resolution Tissue Imaging Using Nanospray Desorption Electrospray Ionization Mass Spectrometry. *Anal. Chem.* **2012**, *84* (19), 8351–8356. https://doi.org/10.1021/ac301909a.

(32) Thomas, M.; Heath, B. S.; Laskin, J.; Dongsheng Li; Liu, E.; Hui, K.; Kuprat, A. P.; Kleese Van Dam, K.; Carson, J. P. Visualization of High Resolution Spatial Mass Spectrometric Data during Acquisition. In *2012 Annual International Conference of the IEEE Engineering in Medicine and Biology Society*; IEEE: San Diego, CA, 2012; pp 5545–5548. https://doi.org/10.1109/EMBC.2012.6347250.

(33) Grgic, A.; Nagornov, K. O.; Kozhinov, A. N.; Michael, J. A.; Anthony, I. G. M.; Tsybin, Y. O.; Heeren, R. M. A.; Ellis, S. R. Ultrahigh-Mass Resolution Mass Spectrometry Imaging with an Orbitrap Externally Coupled to a High-Performance Data Acquisition System. *Anal. Chem.* **2024**, *96* (2), 794–801. https://doi.org/10.1021/acs.analchem.3c04146.

(34) Vandergrift, G. W.; Lukowski, J. K.; Taylor, M. J.; Zemaitis, K. J.; Alexandrov, T.; Eder, J. G.; Olson, H. M.; Kyle, J. E.; Anderton, C. Are Phosphatidic Acids Ubiquitous in Mammalian Tissues or Overemphasized in Mass Spectrometry Imaging Applications? *Analysis & Sensing* **2023**, *3* (5), e202200112. https://doi.org/10.1002/anse.202200112.

(35) Sans, M.; Feider, C. L.; Eberlin, L. S. Advances in Mass Spectrometry Imaging Coupled to Ion Mobility Spectrometry for Enhanced Imaging of Biological Tissues. *Current Opinion in Chemical Biology* **2018**, *42*, 138–146. https://doi.org/10.1016/j.cbpa.2017.12.005.

(36) Jiang, L.-X.; Hernly, E.; Hu, H.; Hilger, R. T.; Neuweger, H.; Yang, M.; Laskin, J. Nanospray Desorption Electrospray Ionization (Nano-DESI) Mass Spectrometry Imaging with High Ion Mobility Resolution. *J. Am. Soc. Mass Spectrom.* **2023**, *34* (8), 1798–1804. https://doi.org/10.1021/jasms.3c00199.

(37) Unsihuay, D.; Yin, R.; Sanchez, D. M.; Yang, M.; Li, Y.; Sun, X.; Dey, S. K.; Laskin, J. High-Resolution Imaging and Identification of Biomolecules Using Nano-DESI Coupled to Ion Mobility Spectrometry. *Analytica Chimica Acta* **2021**, *1186*, 339085. https://doi.org/10.1016/j.aca.2021.339085.

(38) Michael, J. A.; Mutuku, S. M.; Ucur, B.; Sarretto, T.; Maccarone, A. T.; Niehaus, M.; Trevitt, A. J.; Ellis, S. R. Mass Spectrometry Imaging of Lipids Using MALDI Coupled

with Plasma-Based Post-Ionization on a Trapped Ion Mobility Mass Spectrometer. *Anal. Chem.* **2022**, *94* (50), 17494–17503. https://doi.org/10.1021/acs.analchem.2c03745.
(39) Spraggins, J. M.; Djambazova, K. V.; Rivera, E. S.; Migas, L. G.; Neumann, E. K.; Fuetterer, A.; Suetering, J.; Goedecke, N.; Ly, A.; Van De Plas, R.; Caprioli, R. M. High-Performance Molecular Imaging with MALDI Trapped Ion-Mobility Time-of-Flight (timsTOF) Mass Spectrometry. *Anal. Chem.* **2019**, *91* (22), 14552–14560. https://doi.org/10.1021/acs.analchem.9b03612.
(40) McLean, J. A.; Ridenour, W. B.; Caprioli, R. M. Profiling and Imaging of Tissues by Imaging Ion Mobility-Mass Spectrometry. *Journal of Mass Spectrometry* **2007**, *42* (8), 1099–1105. https://doi.org/10.1002/jms.1254.
(41) Trim, P. J.; Henson, C. M.; Avery, J. L.; McEwen, A.; Snel, M. F.; Claude, E.; Marshall, P. S.; West, A.; Princivalle, A. P.; Clench, M. R. Matrix-Assisted Laser Desorption/Ionization-Ion Mobility Separation-Mass Spectrometry Imaging of Vinblastine in Whole Body Tissue Sections. *Anal. Chem.* **2008**, *80* (22), 8628–8634. https://doi.org/10.1021/ac8015467.
(42) Clemis, E. J.; Smith, D. S.; Camenzind, A. G.; Danell, R. M.; Parker, C. E.; Borchers, C. H. Quantitation of Spatially-Localized Proteins in Tissue Samples Using MALDI-MRM Imaging. *Anal. Chem.* **2012**, *84* (8), 3514–3522. https://doi.org/10.1021/ac202875d.
(43) Weigand, M. R.; Unsihuay Vila, D. M.; Yang, M.; Hu, H.; Hernly, E.; Muhoberac, M.; Tichy, S.; Laskin, J. Lipid Isobar and Isomer Imaging Using Nanospray Desorption Electrospray Ionization Combined with Triple Quadrupole Mass Spectrometry. *Anal Chem* **2024**. https://doi.org/10.1021/acs.analchem.3c04705.
(44) Unsihuay, D.; Hu, H.; Qiu, J.; Latorre-Palomino, A.; Yang, M.; Yue, F.; Yin, R.; Kuang, S.; Laskin, J. Multimodal High-Resolution Nano-DESI MSI and Immunofluorescence Imaging Reveal Molecular Signatures of Skeletal Muscle Fiber Types. *Chem. Sci.* **2023**, *14* (15), 4070–4082. https://doi.org/10.1039/D2SC06020E.
(45) Watrous, J.; Roach, P.; Alexandrov, T.; Heath, B. S.; Yang, J. Y.; Kersten, R. D.; van der Voort, M.; Pogliano, K.; Gross, H.; Raaijmakers, J. M.; Moore, B. S.; Laskin, J.; Bandeira, N.; Dorrestein, P. C. Mass Spectral Molecular Networking of Living Microbial Colonies. *Proceedings of the National Academy of Sciences* **2012**, *109* (26), E1743–E1752. https://doi.org/10.1073/pnas.1203689109.
(46) Pessotti, R. de C.; Hansen, B. L.; Zacharia, V. M.; Polyakov, D.; Traxler, M. F. High Spatial Resolution Imaging Mass Spectrometry Reveals Chemical Heterogeneity Across Bacterial Microcolonies. *Anal. Chem.* **2019**, *91* (23), 14818–14823. https://doi.org/10.1021/acs.analchem.9b03909.
(47) Yin, R.; Kyle, J.; Burnum-Johnson, K.; Bloodsworth, K. J.; Sussel, L.; Ansong, C.; Laskin, J. High Spatial Resolution Imaging of Mouse Pancreatic Islets Using Nanospray Desorption Electrospray Ionization Mass Spectrometry. *Anal. Chem.* **2018**, *90* (11), 6548–6555. https://doi.org/10.1021/acs.analchem.8b00161.
(48) Kuo, T.-H.; Chung, H.-H.; Chang, H.-Y.; Lin, C.-W.; Wang, M.-Y.; Shen, T.-L.; Hsu, C.-C. Deep Lipidomics and Molecular Imaging of Unsaturated Lipid Isomers: A Universal Strategy Initiated by mCPBA Epoxidation. *Anal. Chem.* **2019**, *91* (18), 11905–11915. https://doi.org/10.1021/acs.analchem.9b02667.
(49) Lillja, J.; Duncan, K. D.; Lanekoff, I. Determination of Monounsaturated Fatty Acid Isomers in Biological Systems by Modeling MS3 Product Ion Patterns. *J. Am. Soc. Mass Spectrom.* **2020**, *31* (12), 2479–2487. https://doi.org/10.1021/jasms.0c00194.

(50) Mesa Sanchez, D.; Creger, S.; Singla, V.; Kurulugama, R. T.; Fjeldsted, J.; Laskin, J. Ion Mobility-Mass Spectrometry Imaging Workflow. *J. Am. Soc. Mass Spectrom.* **2020**, *31* (12), 2437–2442. https://doi.org/10.1021/jasms.0c00142.
(51) Alexander, W. M.; Ficarro, S. B.; Adelmant, G.; Marto, J. A. Multiplierz v2.0: A Python-Based Ecosystem for Shared Access and Analysis of Native Mass Spectrometry Data. *Proteomics* **2017**, *17* (15–16). https://doi.org/10.1002/pmic.201700091.
(52) Kösters, M.; Leufken, J.; Schulze, S.; Sugimoto, K.; Klein, J.; Zahedi, R. P.; Hippler, M.; Leidel, S. A.; Fufezan, C. pymzML v2.0: Introducing a Highly Compressed and Seekable Gzip Format. *Bioinformatics* **2018**, *34* (14), 2513–2514. https://doi.org/10.1093/bioinformatics/bty046.
(53) Łącki, M. K.; Startek, M. P.; Brehmer, S.; Distler, U.; Tenzer, S. OpenTIMS, TimsPy, and TimsR: Open and Easy Access to timsTOF Raw Data. *J. Proteome Res.* **2021**, *20* (4), 2122–2129. https://doi.org/10.1021/acs.jproteome.0c00962.
(54) Harris, C. R.; Millman, K. J.; van der Walt, S. J.; Gommers, R.; Virtanen, P.; Cournapeau, D.; Wieser, E.; Taylor, J.; Berg, S.; Smith, N. J.; Kern, R.; Picus, M.; Hoyer, S.; van Kerkwijk, M. H.; Brett, M.; Haldane, A.; del Río, J. F.; Wiebe, M.; Peterson, P.; Gérard-Marchant, P.; Sheppard, K.; Reddy, T.; Weckesser, W.; Abbasi, H.; Gohlke, C.; Oliphant, T. E. Array Programming with NumPy. *Nature* **2020**, *585* (7825), 357–362. https://doi.org/10.1038/s41586-020-2649-2.
(55) McKinney, W. Data Structures for Statistical Computing in Python. In *Proceedings of the 9th Python in Science Conference*; Walt, S. van der, Millman, J., Eds.; 2010; pp 51–56.
(56) Virtanen, P.; Gommers, R.; Oliphant, T. E.; Haberland, M.; Reddy, T.; Cournapeau, D.; Burovski, E.; Peterson, P.; Weckesser, W.; Bright, J.; van der Walt, S. J.; Brett, M.; Wilson, J.; Millman, K. J.; Mayorov, N.; Nelson, A. R. J.; Jones, E.; Kern, R.; Larson, E.; Carey, C. J.; Polat, İ.; Feng, Y.; Moore, E. W.; VanderPlas, J.; Laxalde, D.; Perktold, J.; Cimrman, R.; Henriksen, I.; Quintero, E. A.; Harris, C. R.; Archibald, A. M.; Ribeiro, A. H.; Pedregosa, F.; van Mulbregt, P. SciPy 1.0: Fundamental Algorithms for Scientific Computing in Python. *Nat Methods* **2020**, *17* (3), 261–272. https://doi.org/10.1038/s41592-019-0686-2.
(57) Walt, S. van der; Schönberger, J. L.; Nunez-Iglesias, J.; Boulogne, F.; Warner, J. D.; Yager, N.; Gouillart, E.; Yu, T. Scikit-Image: Image Processing in Python. *PeerJ* **2014**, *2*, e453. https://doi.org/10.7717/peerj.453.
(58) *Matplotlib: A 2D Graphics Environment | IEEE Journals & Magazine | IEEE Xplore*. https://ieeexplore.ieee.org/document/4160265 (accessed 2024-04-11).
(59) Lam, S. K.; Pitrou, A.; Seibert, S. Numba: A LLVM-Based Python JIT Compiler. In *Proceedings of the Second Workshop on the LLVM Compiler Infrastructure in HPC*; LLVM '15; Association for Computing Machinery: New York, NY, USA, 2015; pp 1–6. https://doi.org/10.1145/2833157.2833162.
(60) Costa-Luis, C. da; Larroque, S. K.; Altendorf, K.; Mary, H.; richardsheridan; Korobov, M.; Yorav-Raphael, N.; Ivanov, I.; Bargull, M.; Rodrigues, N.; Chen, G.; Dektyarev, M.; mjstevens777; Pagel, M. D.; Zugnoni, M.; JC; CrazyPython; Newey, C.; Lee, A.; pgajdos; Todd; Malmgren, S.; redbug312; Desh, O.; Nechaev, N.; Górny, M.; Boyle, M.; Nordlund, M.; Rothberg, A.; Plavin, A. Tqdm: A Fast, Extensible Progress Bar for Python and CLI, 2024. https://doi.org/10.5281/zenodo.3551211.
(61) Adusumilli, R.; Mallick, P. Data Conversion with ProteoWizard msConvert. In *Proteomics: Methods and Protocols*; Comai, L., Katz, J. E., Mallick, P., Eds.; Springer: New York, NY, 2017; pp 339–368. https://doi.org/10.1007/978-1-4939-6747-6_23.

(62) Unsihuay, D.; Su, P.; Hu, H.; Qiu, J.; Kuang, S.; Li, Y.; Sun, X.; Dey, S. K.; Laskin, J. Imaging and Analysis of Isomeric Unsaturated Lipids through Online Photochemical Derivatization of Carbon–Carbon Double Bonds**. *Angewandte Chemie International Edition* **2021**, *60* (14), 7559–7563. https://doi.org/10.1002/anie.202016734.
(63) Unsihuay, D.; Yin, R.; Sanchez, D. M.; Yang, M.; Li, Y.; Sun, X.; Dey, S. K.; Laskin, J. High-Resolution Imaging and Identification of Biomolecules Using Nano-DESI Coupled to Ion Mobility Spectrometry. *Analytica Chimica Acta* **2021**, *1186*, 339085. https://doi.org/10.1016/j.aca.2021.339085.
(64) Jiang, L.-X.; Polack, M.; Li, X.; Yang, M.; Belder, D.; Laskin, J. A Monolithic Microfluidic Probe for Ambient Mass Spectrometry Imaging of Biological Tissues. *Lab Chip* **2023**, *23* (21), 4664–4673. https://doi.org/10.1039/D3LC00637A.
(65) Nguyen, S. N.; Liyu, A. V.; Chu, R. K.; Anderton, C. R.; Laskin, J. Constant-Distance Mode Nanospray Desorption Electrospray Ionization Mass Spectrometry Imaging of Biological Samples with Complex Topography. *Anal. Chem.* **2017**, *89* (2), 1131–1137. https://doi.org/10.1021/acs.analchem.6b03293.
(66) Nguyen, S. N.; Sontag, R. L.; Carson, J. P.; Corley, R. A.; Ansong, C.; Laskin, J. Towards High-Resolution Tissue Imaging Using Nanospray Desorption Electrospray Ionization Mass Spectrometry Coupled to Shear Force Microscopy. *J. Am. Soc. Mass Spectrom.* **2018**, *29* (2), 316–322. https://doi.org/10.1007/s13361-017-1750-8.
(67) Laskin, J.; Heath, B. S.; Roach, P. J.; Cazares, L.; Semmes, O. J. Tissue Imaging Using Nanospray Desorption Electrospray Ionization Mass Spectrometry. *Anal Chem* **2012**, *84* (1), 141–148. https://doi.org/10.1021/ac2021322.
(68) Yin, R.; Burnum-Johnson, K. E.; Sun, X.; Dey, S. K.; Laskin, J. High Spatial Resolution Imaging of Biological Tissues Using Nanospray Desorption Electrospray Ionization Mass Spectrometry. *Nat Protoc* **2019**, *14* (12), 3445–3470. https://doi.org/10.1038/s41596-019-0237-4.
(69) Schwartz, J. C.; Zhou, X.-G.; Bier, M. E. Method and Apparatus of Increasing Dynamic Range and Sensitivity of a Mass Spectrometer. US5572022A, November 5, 1996. https://patents.google.com/patent/US5572022A/en (accessed 2024-04-22).